Acousto-optic Tuneable Filter design for marine plastic debris detection

Samuel Dupont[1], Emmanuel Dekemper[2], Jurgen Van-Hamel[3,4], Jean-Claude Kastelik[1]

[1] *IEMN site de Valenciennes, INSA HdF, Université Polytechnique Hauts-de-France, France*
[2] *Royal Belgian Institute for Space Aeronomy (BISA), Brussels, Belgium*
[3] *Technical University of Delft (TU Delft), Delft, The Netherlands*
[4] *Electronic Circuits and Systems, KU Leuven, Geel, Belgium*

This paper is a revised version of the authors' submitted manuscript that was peer-reviewed by at least two anonymous reviewers.

Abstract

Marine plastic pollution represents one of the most pressing environmental challenges of the contemporary era. Despite extensive research, the formation, transformation, and short-term dynamics of floating plastic debris remain inadequately understood, primarily due to insufficient high-resolution spatiotemporal observations. Furthermore, conventional space-based multispectral sensors, while valuable for ocean monitoring, lack the spectral and polarimetric capabilities required for effective plastic detection.

To address these limitations, this study investigates the potential of hyperspectral imaging in the Short-Wave InfraRed range, focusing on the development of a tuneable acousto-optic filter optimized to exploit plastic-specific spectral signatures. The proposed approach integrates advanced spectral indices and polarimetric measurement requirements to enhance discrimination between plastics and their marine surroundings under complex environmental conditions. This article outlines the theoretical framework for filter design and evaluates its expected performance, offering a promising pathway toward improved remote sensing of marine plastic debris.

Keywords: *Acousto-optic filters, spectral imaging, optical polarization analysis*

1. Introduction

Ocean plastic pollution is a major environmental challenge [1, 4]. Plastic accumulations grow continuously from rivers, coasts, and maritime activities, transported by currents, wind, and waves. While large-scale plastic movement is well-studied, the short-term dynamics and transformation mechanisms of these accumulations remain unclear due to a lack of high-resolution, global observations.

Current space-based monitoring, though useful for ocean surface data, is not optimized for plastic detection. Most remote sensing methods use limited spectral bands, making it difficult to distinguish plastics from seawater or organic matter. Additionally, plastics undergo physical and chemical alterations in the marine environment, modifying their optical properties and spectral signatures—factors often overlooked in detection algorithms, leading to inaccuracies. High-resolution imaging spectroscopy represents a promising approach in space-based observation to address the current limitations in marine plastic debris detection. The acquisition of detailed spectral data across a broad range of Short-Wave InfraRed (SWIR) wavelengths is essential, as this spectral region exhibits distinctive reflectance characteristics of plastics [5–10].

The Tuneable Acousto-Optic Filter (AOTF) [11-13] emerges as a highly adaptable instrument for this purpose, enabling rapid and electronic selection of narrow spectral bands without mechanical parts. AOTF devices are extensively utilized across multiple industrial sectors, including instrumentation e.g., spectroscopy, hyperspectral imaging and polarimetric imaging [14-17]. Their applications span diverse fields such including airborne and space missions [17-23]. Hence, AOTF suitability for remote sensing applications has been widely demonstrated and its established use in space-based systems further underscores its potential. By targeting specific wavelengths, AOTF technology facilitates the development of spectral indices, thereby potentially enhancing the discrimination between plastics and their surrounding marine environment.

This article synthesizes the spectral imaging requirements for marine plastic debris analysis, reviews the design methodology of the AOTF, and presents the key performance parameters essential for its application in marine plastic debris detection.

2. Requirements

Satellite remote sensing literature review enables to define the early instrumentation requirements. The International Ocean Colour Coordination Group (IOCCG) has organized research within the field of ocean colour science, including a specific focus on the remote sensing of marine litter. Through its contributions, the IOCCG has produced several

Corresponding author: samuel.dupont@uphf.fr.

publications that review the current state of measurement techniques for marine litter and plastic debris [20]. Additionally, these works synthesize key outstanding scientific questions [6] and establish the optimal instrumental requirements necessary to address these challenges [6, 24]. The analysis of the reflectance of plastics of different colours in the SWIR domain has shown that the different materials have similar absorption spectra in this band [25, 26]. Recent studies have explored the use of light scattering (de)polarization on macroplastics [27]. Beyond spectral absorption, it has been sketched that measuring the Degree of Linear Polarization (DoLP) can enhance the detectability of plastic surfaces.

The review of the existing literature has allowed to establish a set of technical specifications essential for optimizing the detection of marine plastic debris through remote sensing [25]. The recommended instrument parameters include a ground sampling resolution of 10 meters, enabling high spatial detail; a spectral range extending from 850 nm to 1750 nm, which captures the key reflectance features of plastics; a spectral resolution of 10 nm, ensuring precise spectral absorption band resolution; and the acquisition of four linear polarization measurements, which are necessary to compute the DoLP index, a critical metric for distinguishing plastic materials from their surrounding environment.

Building upon these specifications, the development of an AOTF specifically designed for marine plastic debris detection has been initiated. This technology, known for its adaptability and rapid spectral selection capabilities, holds significant promise for enhancing the accuracy and efficiency of plastic detection in marine ecosystems. By integrating these parameters, the AOTF-based system aims to address the current limitations in remote sensing and provide a robust tool for monitoring and mitigating plastic pollution in the world's oceans.

3. AOTF design process

A Tuneable Acousto-Optic Filter enables the selective extraction of a specific optical wavelength from a polychromatic light beam by applying a corresponding acoustic frequency [8]. This relationship is governed by the Bragg synchronism conditions, which define the interaction between light and sound waves within the medium with elastooptical properties. Bragg conditions describe the geometric and frequency-dependent criteria by which the acousto-optic interaction occurs. In the context of AOTFs, these conditions ensure that a specific optical wavelength is diffracted (or "selected") by an acoustic wave. Interaction is governed by two key principles: conservation of momentum and conservation of energy.

The criteria for conserving momentum state that the wave vectors of incident light, diffracted light, and acoustic wave must satisfy a vector relationship. Whereas the conservation of energy criteria express that the frequency of the diffracted light must correspond to the sum (or difference) of the frequency of the incident light and the acoustic frequency (depending on the type of interaction: shifted up or down).

In anisotropic (birefringent) acousto-optic materials, such as Paratellurite (TeO_2), the non-collinear interaction couples the incident and diffracted beams, which are orthogonally polarized. The most common configuration for this interaction is known as Narrow Phase Matching (NPM). In this setup, a polychromatic, linearly polarized incident beam enters the Paratellurite crystal at normal incidence. An ultrasonic wave, generated by a piezoelectric transducer, diffracts the wavelength associated with the applied acoustic frequency. The intensity of the diffracted beam is directly proportional to the acoustic power, and under ideal synchronism conditions, it is theoretically possible to achieve a 100% transfer of optical energy from the incident beam to the diffracted beam, provided sufficient acoustic power is applied.

Expressed mathematically, the Bragg condition relates the key parameters of this interaction, including: λ_0: the optical wavelength, θ_i: the angle of the incident optical beam, f: the acoustic frequency, θ_a: the acoustic cut angle. At synchronism, the Bragg condition is expressed by Eq. 1:

$$\boldsymbol{k_i} \pm \boldsymbol{K} = \boldsymbol{k_d} \tag{1}$$

with: $k_{i/d} = 2\pi n_{i/d}/\lambda_0$ the incident (/diffracted) optical wave vectors (n: refractive index) and $K = 2\pi f/V$ the acoustic wave vector, as illustrated by fig. 1. The figure illustrates the ordinary to extraordinary case when the incident optical radiation is coupled to the ordinary wave, an extraordinary to ordinary diffraction case also exists. The plane of interaction, as illustrated in Fig. 1, exhibits high acoustic slowness, thereby facilitating efficient diffraction.

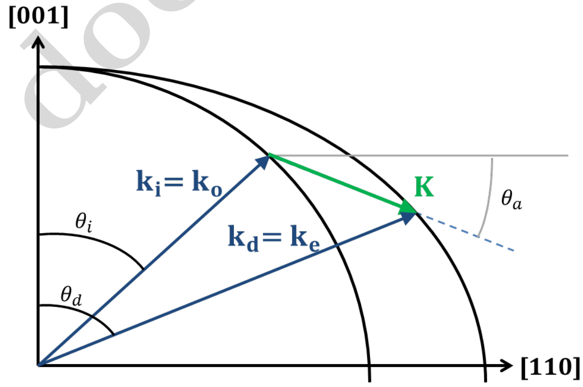

Figure 1. Ordinary to extraordinary interaction in TeO_2.

The exploitation of the Bragg interaction geometry leads to a system of two equations, Eq. (2):

$$\begin{cases} \dfrac{2\pi.n_o(\theta_i)}{\lambda_0}\cos\theta_i - \dfrac{2\pi}{K}\sin\theta_a = \dfrac{2\pi.n_e(\theta_d)}{\lambda_0}\cos\theta_d \\ \dfrac{2\pi.n_o(\theta_i)}{\lambda_0}\sin\theta_i + \dfrac{2\pi}{K}\cos\theta_a = \dfrac{2\pi.n_e(\theta_d)}{\lambda_0}\sin\theta_d \end{cases} \tag{2}$$

Given the wavelength-dependent refractive index of paratellurite (TeO_2) and the gyrotropic effects, which induce a rotation of the polarization plane during optical wave propagation, an analytical solution for this system becomes intractable. Consequently, a numerical approach is required to accurately model the interaction between acoustic and optical waves, ensuring precise prediction of the diffraction conditions. The dependence of the Bragg matching conditions on the interaction parameters can then be systematically characterized.

When the interaction deviates from the ideal Bragg matching conditions, the diffraction efficiency significantly diminishes. To quantify this effect, the wave vector mismatch (Δk) is introduced, as depicted in Fig. 2. By incorporating the interaction length (L), this mismatch translates into a phase detuning (ΔΦ), or phase mismatch parameter, which must be accounted for in the analysis of acousto-optic diffraction performance.

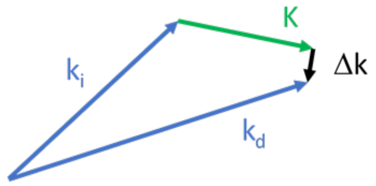

Figure 2. Wave vector diagram with mismatch.

The overall impact of phase detuning on interaction efficiency is quantitatively described by the well-known efficiency expression, η, as given in Eq. 3:

$$\eta = \frac{P}{P_0}\frac{\sin^2\left(\frac{\pi}{2}\sqrt{\frac{P}{P_0}+\left(\frac{\Delta\Phi}{\pi}\right)^2}\right)}{\frac{P}{P_0}+\left(\frac{\Delta\Phi}{\pi}\right)^2} \qquad (3)$$

In Eq. 3, P denotes the applied acoustic power, while P_0 represents the threshold acoustic power required to achieve 100% diffraction efficiency. A systematic analysis of diffraction efficiency as a function of key interaction parameters provides insights for characterizing the performance metrics of the AOTF.

4. Evaluation of AOTF characteristics

Here we sketch the theoretical performances of an AOTF.

4.1 Simultaneous diffraction

Fig. 3 depicts the evolution of the acoustic frequency at synchronism as a function of the optical incident angle. The red curve corresponds to a diffraction from ordinary to extraordinary mode and the blue curve is the opposite case.

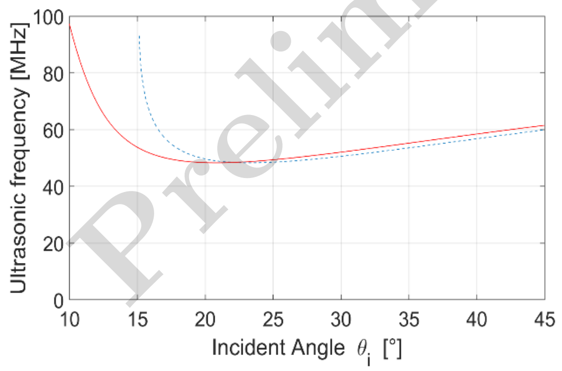

Figure 3. Evolution of acoustic frequency as a function of optical incident angle, with: θ_a = 10° and λ_o = 1450 nm.

The two curves interact at one point which corresponds to the simultaneous diffraction conditions from ordinary to extraordinary mode and from extraordinary to ordinary [13]. It is possible to exploit this operation conditions to create a system with polarimetric analysis capabilities. In the following developments, this particular operation point is aimed at: the simultaneous diffraction.

4.2 Acoustic frequency

The Bragg acoustic frequency f required for simultaneous diffraction exhibits a positive correlation with the acoustic cut angle. As illustrated in Fig. 4, f increases from 23 MHz at an acoustic cut angle of 5° to 60 MHz at 12°. These cut angles are typically employed in practical AOTF designs. Higher angles are generally avoided due to the associated decrease in diffraction efficiency; lower cuts also as they are more sensitive to gyrotropy effect. The corresponding RF frequencies found are usual for ultrasonic transducers.

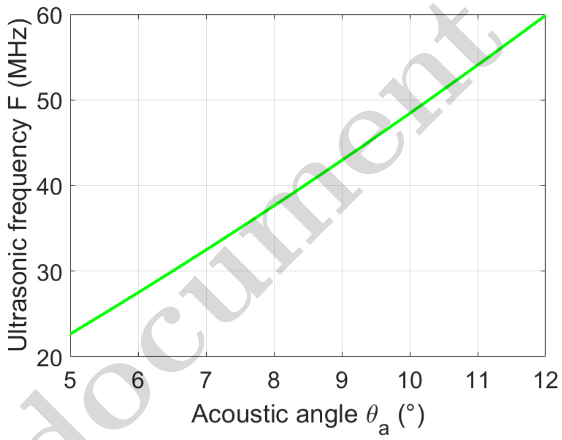

Figure 4. Evolution of acoustic frequency as a function of acoustic cut with λ_o = 1450nm.

The observation of plastic debris would benefit from spectroscopic analysis in the SWIR. Fig. 5 is showing the evolution of the ultrasonic frequency for wavelength comprised between 750 nm to 1850 nm, covering the preliminary band highlighted by the literature review.

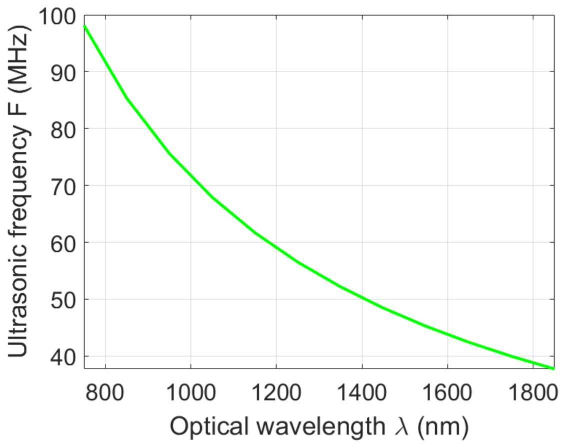

Figure 5. Evolution of acoustic frequency as a function of wavelength, acoustic cut considered: 10°.

For the depicted curve corresponding to an acoustic cut angle of 10°, the resulting radio frequency (RF) bandwidth spans from 38 MHz to nearly 100 MHz. To achieve transducer matching across a bandwidth exceeding one octave, a switched RF architecture may be employed. Each switched segment covers less than one octave; when combined, they yield an extended usable frequency range [28]. The principal drawback is approximately 3 dB attenuation of the RF signal, which should be accounted for in the system design. Actually, obtaining extended tuning range is possible [29], however it could be interesting to reduce the operation band of the spectro-polarimetric imaging device: the RF matching over a reduced band is simpler; moreover, the availability of imaging detectors is greater, so does efficient commercially available optical anti-reflection coatings. For these reasons, a spectral range extending from 1100 nm to 1800 nm is preferred, as it facilitates the evolution of acoustic frequencies within a single octave.

4.3 Optical filter resolution

The optical bandwidth $\Delta\lambda$ of an AOTF is defined according to a minimum efficiency criterion: usually 50%, this affects the spectral resolution of the instrument in which it is placed. $\Delta\lambda$ is proportional to λ^2 and inversely proportional to the interaction length L [30]. Hence, the bandwidth may be maintained at a constant level over an extended range of wavelength by employing a modified transducer equipped with multiple electrodes, which enables adjustment of the parameter L through selective activation or deactivation of the individual transducers [13]. But, as a first design, we focus on a simple unique electrode device. As a consequence, it is expected that the filter resolution increases with wavelength. The simulated bandwidth as a function of wavelength is plotted in Fig. 6, for different acoustic cuts.

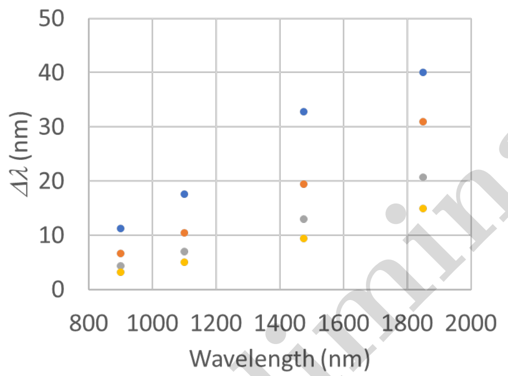

Figure 6. AOTF bandwidth vs. wavelength for various acoustic cuts, with L = 10 mm.

As illustrated by Fig. 6, higher wavelengths correspond to greater bandwidths. The evolution is scalable by adjusting the interaction length. As an example, with an acoustic cut of 8° and an interaction length of 15 mm, $\Delta\lambda$ would diminish down to 20 nm at λ = 1800 nm.

4.4 AOTF efficiency

The efficiency of acousto-optic (AO) interaction is characterized by the canonical acoustooptic figure of merit M_2:

$$M_2 = p^2 n^6 / (\rho V^3) \quad (4)$$

where p is the effective photoelastic constant, n the refractive index, ρ the medium density and V the sound velocity.
The higher slowness, $1/V$, is experienced in the [110] direction of interaction plane, a plot of the relative M_2 index with respect to maximum value is depicted in Fig. 7. Usual practical cuts are maintained below 12° to ensure relative M_2 to be higher than 0,5.

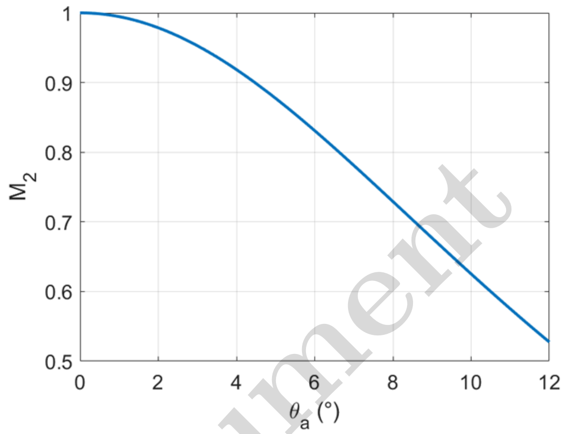

Figure 7. AOTF relative figure of merit M_2.

4.5 Choice of an acoustic cut

Paratellurite being an anisotropic media, the choice of the acoustic cut affects the performances of the AOTF. The higher slowness corresponding to efficient diffraction are found for the lower cuts in the interaction plane considered. However, it is well known that this configuration also results in a more pronounced effect of gyrotropy. Higher cuts are also prone to an increase of acoustic loss and obliquity (inclination of energy flow with respect to wavevector). Finally, the acoustic cut should be sufficiently high to avoid gyrotropic effects and achieve narrow spectral selectivity, yet maintained sufficiently low to minimize acoustic loss and obliquity. An acoustic cut of 8° would be a good compromise as it maintains a sufficiently high diffraction efficiency (relative M_2 > 0,75) and allows to obtain resolution close to the 10 nm bandwidth value underlined by the literature review.

4.6 AOTF theoretical performances

Table 1 summarizes the theoretical performance of an AOTF suitable for meeting the specifications of marine plastic litter analysis, as expressed in literature review; and operating a simultaneous diffraction of ordinary and extraordinary modes.

Table 1. AOTF key parameters.

Parameter	Value
Acoustic cut	8°
Transducer length	15 mm
Optical operation band	1100-1800 nm
RF operation band	30-50 MHz
Optical resolution	7nm @ 1100nm 20nm @ 1800nm

5. Conclusion

In this paper we evaluated the potential of AOTF technologies to satisfy generic requirements for marine plastic debris analysis. We analyzed the physical constraints of acousto-optic interaction at the design stage to outline the expected AOTF performance. By examining Bragg phase-matching for ordinary-to-extraordinary and extraordinary-to-ordinary conversions in anisotropic crystals as functions of acoustic cut, wavelength, RF frequency, and optical incidence angle, we derived achievable operating characteristics. The choice of the crystal acoustic cut provides a means to set the operating point; a trade-off between diffraction efficiency and optical resolution led to an acoustic cut of 8°. The predicted AOTF performance meets the target metrics: spectral resolution below 20 nm and a relative figure-of-merit $M_2 \geq 0.75$.
The AOTF characteristics will enable to evaluate the design of an instrument with deployable optics to be embedded on the Very Low Earth Orbit (VLEO; with altitudes below 400 km) platform.

6. Acknowledgments

The authors acknowledge the support from the European Space Agency under the OSIP program (Open Space Innovation Platform) PLASMO.

References

[1] P.G. Ryan, C.J. Moore, J.A. Van Franeker, and C.L. Moloney, "Monitoring the abundance of plastic debris in the marine environment", *Philosophical Trans. of the Royal Society B: Biological Sciences*, vol. 364, no. 1526, pp. 1999 – 2012, 2009.

[2] Y. Laberge, "Review: plastic soup: an atlas of ocean pollution", *Electronic Green Journal*, vol. 1, no. 43, 1A–2, 2020.

[3] I. Issifu, and U.R. Sumaila, "A review of the production, recycling and management of marine plastic pollution," *Journal of Marine Science and Engineering*, vol. 8, no. 11, 2020.

[4] L. Biermann, D. Clewley, V. Martinez-Vicente, and K. Topouzelis, "Finding plastic patches in coastal waters using optical satellite data", *Scientific Reports*, vol. 10, 2020.

[5] S.P. Garaba, and H.M. Dierssen, "An airborne remote sensing case study of synthetic hydrocarbon detection using short wave infrared absorption features identified from marine-harvested macro- and microplastics", *Remote Sensing of Environment*, vol. 205, pp. 224 – 235, 2018.

[6] V. Martínez-Vicente, et al., "Measuring marine plastic debris from space: initial assessment of observation requirements", *Remote Sensing*, vol. 11, no. 20, 2443, 2019.

[7] S.P. Garaba, et al. "Sensing ocean plastics with an airborne hyperspectral shortwave infrared imager", *Environmental Science & Technology*, vol. 52, no. 20, pp. 11699 – 11707, 2018.

[8] MANTSEVICH, Sergey N. Method of plastic type definition by characteristic spectral features in the near-IR range. *Applied optics*, vol. 65, no 6, p. 1745-1752, 2026.

[9] MENDOZA, A., KORTABERRIA, G., CARRERO, D., *et al.* Industrial optical sorting for marine plastic litter management. *Waste Management Bulletin*, vol. 2, no 4, p. 102-107, 2024.

[10] YANG, Jian, XU, Yu-Peng, CHEN, Pu, *et al.* Combining spectroscopy and machine learning for rapid identification of plastic waste: Recent developments and future prospects. *Journal of Cleaner Production*, vol. 431, p. 139771, 2023.

[11] I. C. Chang "Tunable Acousto-Optic Filters: An Overview," *Optical Engineering*, vol. 16, no. 5, 165455, 1977.

[12] E. Dekemper, et al. "Tunable acousto-optic spectral imager for atmospheric composition measurements in the visible spectral domain", *Appl. Opt.* 51, pp. 6259–67, 2012.

[13] S. Dupont, J.C. Kastelik, J. VanHamel, "Design and testing of a multi-electrode apodised acousto-optic filter for arbitrary polarized light", *Applied optics*, *63*(10), pp. 2487-2493, 2024.

[14] N. Gat, "Imaging spectroscopy using tuneable filters: a review", *Proc. SPIE*, vol. 4056, pp. 50–64, 2000.

[15] V.B. Voloshinov, K.B. Yushkov, and B.B.J. Linde, "Improvement in performance of a TeO_2 acousto-optic imaging spectrometer", *Journal of Optics A: Pure and Applied Optics*, vol. 9, pp. 341, 2007.

[16] N. Gupta, "Biosensors technologies: acousto-optic tuneable filter-based hyperspectral and polarization imagers for fluorescence and spectroscopic imaging", *Biosensors and Biodetection*, vol. 503, pp. 293–305, 2008.

[17] C. Pannell, "Recent advances in acousto-optic tunable filters for hyperspectral imaging with real-time spectral unmixing", *CLEO: Applications and Technology*, AF1J, 62013, 2013.

[18] W. Hayden Smith and K. Smith, "A polarimetric spectral imager using acousto-optic tunable filters", *Experimental Astronomy*, vol. 1, pp. 329–343, 1990.

[19] N.J. Chanover, D.A. Glenar, and J.J. Hillman, "Multispectral near-IR imaging of Venus nightside cloud features", *Journal of Geophysical Research: Planets*, vol. 103, no. E13, pp. 31335–31348, 1998.

[20] O. Korablev, J.-L. Bertaux, A. Grigoriev, E. Dimarellis, Y. Kalinnikov, A. Rodin, C. Muller, and D. Fonteyn, "An AOTF-based spectrometer for the studies of Mars atmosphere for Mars Express ESA mission", *Advances in Space Research*, vol. 29, pp. 143–150, 2002.

[21] V. Leroi, J.-P. Bibring, and M. Berthe, "Micromega/IR: design and status of a near-infrared spectral microscope for in situ analysis of Mars samples",

Planetary and Space Science, vol. 57, pp. 1068–1075, 2009.

[22] J. Wang, Z. He, R. Shu, et al., “Visible and near-infrared imaging spectrometer aboard Chinese Chang’E 3 spacecraft”, *Optical Payloads for Space Missions*, pp. 121–139, 2015.

[23] E. Dekemper, D. Fussen, B. Van Opstal, et al., “ALTIUS: a spaceborne AOTF-based UV–VIS–NIR hyperspectral imager for atmospheric remote sensing”, *Sensors, Systems, and Next-Generation Satellites XVIII*, Proc. SPIE, pp. 151–160, 2014.

[24] A. Cózar *et al.*, “Proof of concept for a new sensor to monitor marine litter from space,” *Nat Commun*, vol. 15, no. 1, pp. 4637, June 2024.

[25] S. P. Garaba and T. Harmel, “Top-of-atmosphere hyper and multispectral signatures of submerged plastic litter with changing water clarity and depth,” *Opt. Express, OE*, vol. 30, no. 10, pp. 16553–16571, May 2022.

[26] M. Moshtaghi, et al., “Spectral reflectance of marine macroplastics in the VNIR and SWIR measured in a controlled environment,” *Sci. Rep.*, vol. 11, no. 1, pp. 5436, 2021.

[27] A. De Fockert *et al.*, “Assessing the detection of floating plastic litter with advanced remote sensing technologies in a hydrodynamic test facility,” *Sci Rep*, vol. 14, no. 1, pp. 25902, Oct. 2024.

[28] J. Vanhamel, et al. "Design of a radio frequency compensation system, using the electrical characterisation of a multi-transducer acousto-optical tunable filter", *10th Convention of the European Acoustics Association Forum Acusticum*, pp. 6355-6360, 2023.

[29] N. Gupta and V.B. Voloshinov, "Development and characterization of two-transducer imaging acousto-optic tunable filters with extended tuning range," *Appl. Opt.*, vol. 46, pp. 1081-1088, 2007.

[30] G. Georgiev, D. A. Glenar, and J. J. Hillman, “Spectral characterization of acousto-optic filters used in imaging spectroscopy,” *Applied optics*, vol. 41, no. 1, pp. 209–217, 2002.